Mathematical Biosciences and Engineering

Mathematical Biosciences and Engineering, 16(4): 3144–3168.
DOI: 10.3934/mbe.2019156
Received: 07 February 2019
Accepted: 02 April 2019
Published: 11 April 2019

http://www.aimspress.com/journal/MBE

Research article

Numerical analysis on the shear behavior of single-keyed dry joints in precast high-strength concrete segmental bridges

Haibo Jiang, Shaodi Wang, Zhuangcheng Fang, Gongfa Chen* and Jiahang Li

School of Civil and Transportation Engineering, Guangdong University of Technology, Guangzhou Higher Education Mega Center, Guangzhou, 510006, China

*** Correspondence:** Email: gongfa.chen@gdut.edu.cn; Tel: +8613662483527.

Abstract: The structural behavior of precast concrete segmental bridges (PCSBs) is affected by the joints between the concrete segments. In this study, a numerical model was established to investigate the direct shear behavior of single-keyed dry joints in PCSBs. The numerical model was validated by the full-scale test results published by the authors. It was found that the numerical results of the joints, such as the ultimate shear load, cracking pattern, and load-displacement curves, matched the test results well. The validated numerical model was further used for extending parametric studies. The factors affecting the shear behavior of single-keyed dry joints include the confining pressure, concrete strength, and key depth. It was found that the ultimate shear capacity increased about 121% when the confining pressure increased from 0.1 to 3.0 MPa, it was very low under confining pressure of 0.1 MPa; it increased about 44% when the concrete strength increased from C40 to C100; it increased about 203% when the key depth increased from 15 to 40 mm. However, the ultimate shear capacity decreased about 20% when the key depth increased from 40 to 60 mm, hence 40 mm was recommended for the design depth of the single-keyed dry joints in PCSBs. Finally, the parametric analysis results were compared with the AASHTO specification. When the key depth was 35, 40 and 45 mm, the AASHTO specification conservatively predict the shear strength capacity of single-keyed dry joints.

Keywords: precast high-strength concrete segmental bridges; single-keyed dry joints; concrete strength; confining pressure; key depth; numerical analysis

1. Introduction

The precast concrete segmental bridges (PCSBs) have advantages of easy construction, comprehensive serviceability and low lifecycle cost, which may solve a range of problems in bridge design, construction, and maintenance [1]. The joints between the PCSBs are of critical importance, which largely affects the overall structural behavior of PCSBs. There are epoxied joints and dry joints used in PCSBs. Though the PCSBs with dry joints may be susceptible to durability problems, they get more and more popular owing to their easy construction. Epoxied joints perform better than dry joints in terms of the durability and ultimate shear capacity [2]. However, it has been found that epoxied joints failed in a brittle manner, which is not desirable in structural design. Turmo et al. pointed out that, when possible, the use of epoxied joints should be avoided because dry joints is time-savings [3].

Recently, the shear behavior of joints in PCSBs has been investigated by both the experimental and theoretical approaches. Experimental results indicated that the failure model of the shear keys was concrete cracking along the joint with the keys' shearing off. The shear strength of dry joints increased with the confining pressure (i.e., the prestress applied on the joint holding the male and female parts together) and concrete strength [4]. Based on the experimental results, it has been concluded that the most significant parameters that influence the shear behavior of the keyed dry joints were the prestress, shape of the keys, number of the keys, concrete materials [5,6]. Meanwhile, a lot of achievements have been made in the theoretical research on the shear performance of the joints [7–9]. Based on the existing formula of the direct shear bearing capacity of the keyed joints and the shear theory of the concrete bridge, the formula for the shear strength of single-keyed dry joints in the AASHTO specification was proposed by adopting the Mohr's circle theory to analyze the keyed joints and combining with assuming a compression strut angle of 45 degrees and data fitting [7]. The arch effect, which illustrates the structural response to the vertical loads, can be explained by the shear flow mechanism in segmental concrete structures [8]. Additionally, the AASHTO specification overestimates the shear strength of multiple-keyed dry joints and underestimates the shear strength of single-keyed dry joints by the shear test with the corresponding formula [9].

Though there are various experimental and theoretical studies on shear keys reported, numerical analyses on shear behavior of keyed joints are very scare, especially for high-strength concrete. Finite element (FE) modeling of the joints can provide a useful insight into the structural performance of the joints and compensate the lack of the full-scale tests on the joints. Recent developments in computers and FE method make it possible to analyze structures with different material properties, different number of keys (single-keyed and multi-keyed), and different types of joints (flat joints, dry joints, and epoxied joints) [10–12]. The calculated results were in good agreement with the experimental results and demonstrated that the observation of sequential failure of multi-keyed dry joints from the lower to upper keys.

The high-strength concrete C40–C100 has potential application in PCSBs to reduce the weight and facilitate the assembly on site. However, the shear failure mechanism of single-keyed dry joints in precast high-strength concrete segmental bridges (PHCSBs) has not been widely studied. The confining pressure in the previous exploration was usually large than 0.5 MPa. Shamass et al. studied the keyed dry joints under the confining pressure greater than 3.0 MPa by numerical analysis [13]. It was necessary to use the numerical method to study the shear behavior of the joints under the

confining pressure less than 0.5 MPa, due to its difficulty to implement low confining pressure in the test. It is well accepted that the shear strength of keyed dry joints is attributed to two different mechanisms. The first one depends on the friction resistance between the surfaces, which slides against each other. This resistance is proportional to the confining pressure. The second mechanism represents the support of the castellated shear keys, which behave like small plain concrete corbels when they are in contact. The direct shear failure surface of the keyed dry joints is shown in Figure 1. The bottom of joints is more likely to open in low confining pressure, which decreases the shear capacity of joints because of the weakening of both friction and shear resistance. Besides, the pre-stress applying in fabrication and assembling, or the construction error at prefabrication, will also lead to the low confining pressure on the shear keyed joints. This has made a great influence in construction of bridge engineering, yet few study focused on it. In this study, a numerical model was proposed and validated by the experimental results published by the authors, it was further used for parametric studies on the factors affecting the shear behavior of single-keyed dry joints, which includes the confining pressure, concrete strength and key depth. Finally, the parametric analysis results were compared with the calculations based on the AASHTO specification.

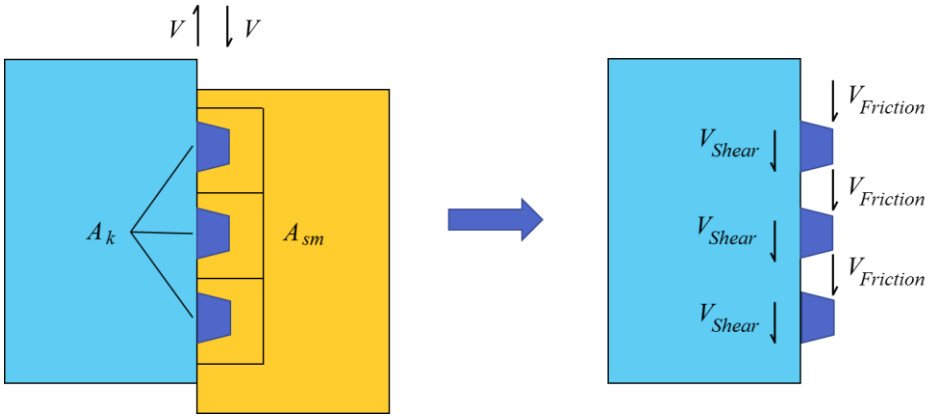

Figure 1. The direct shear failure surface of keyed dry joints.

2. Numerical model

2.1. Concrete damage plastic model

The concrete damage plasticity (CDP) model was chosen in the current study for simulating concrete. It allows the definition of inelastic and damage characteristics of concrete in compression and tension. The compressive damage parameter d_c needs to be defined at each inelastic strain level. It ranges from 0, for an undamaged material, to 1, when the material has totally lost its loadbearing capacity. The value d_c is obtained only for the descending branch of the stress-strain curve of concrete in compression in Figure 2. Similar to the case of compression, the tensile damage parameter d_t needs to be defined with the cracking strain. The d_t is valid only at the descending branch of the stress-strain curve of concrete in tension in Figure 3. The dilation angle, flow potential

eccentricity, and viscosity parameter of the CDP model were 36, 0.1, and 0.0015 [13], respectively; the ratio of the strength in the biaxial state to the strength in the uniaxial state of concrete was $f_{b0} / f_{c0} = 1.16$; and the ratio of the second stress invariant on the tensile meridian plane was K_c = 0.667.

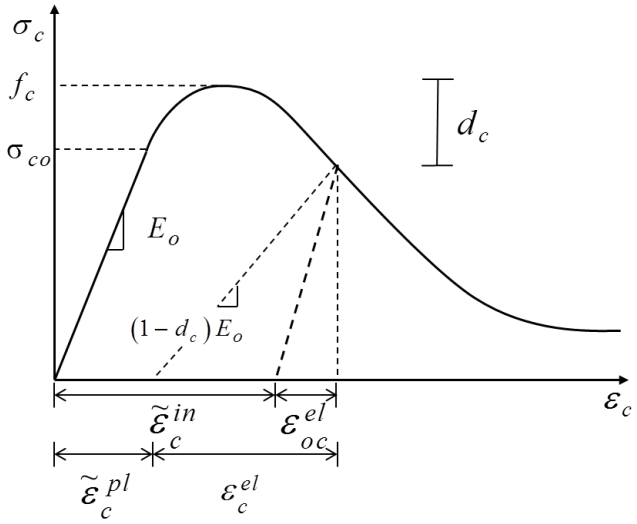

Figure 2. CDP model in compression.

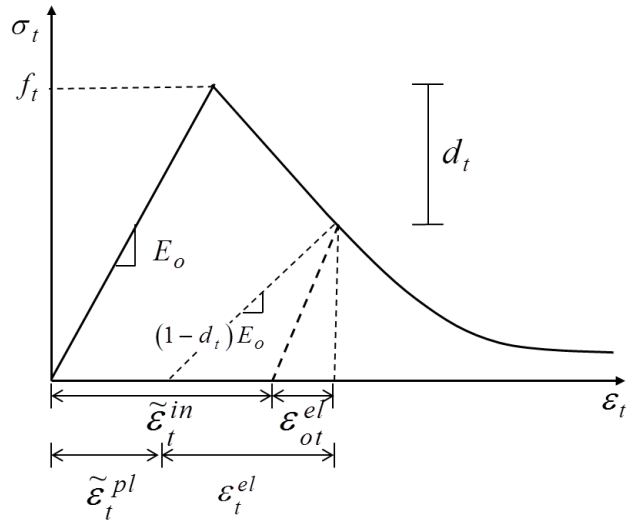

Figure 3. CDP model in tension.

As CDP cannot describe the initiation and development of fractures, to simulate the fracture of concrete, it was assumed that fracture was initiated when the tensile strain ε_0 was larger than 10 times of standard concrete failure strain ε_{cr}, as shown in Figure 4. When reaching the ultimate tensile strain, the concrete have lost the resistance to cracking [14].

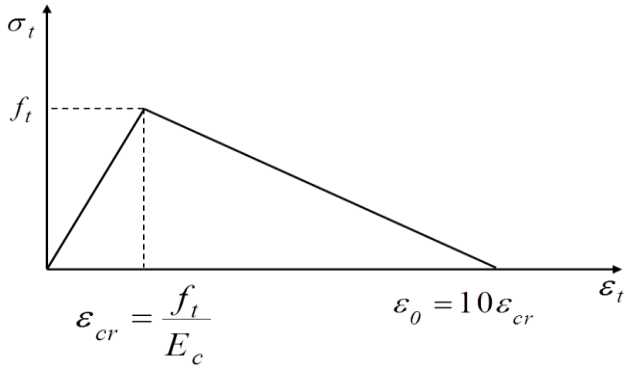

Figure 4. Tensile $\sigma - \varepsilon$ curve of concrete: linear representation.

2.2. Stress-strain curve of concrete under uniaxial compression

As mentioned previously, the CDP model was selected for simulating concrete cracking and crack propagation. To use this approach, stress-strain relationships for concrete in compression and post-failure in tension are required. In this study, for concrete with strength C40–C80,the complete $\sigma_c - \varepsilon_c$ curve specified by Chinese code for the design of concrete structures (GB 50010-2010) was adopted for concrete under compression [15], which suggests the following expression:

$$\sigma = (1 - d_c)\, E_c \varepsilon \tag{1}$$

$$d_c = \begin{cases} 1 - \dfrac{\rho_c n}{n - 1 + x^n} & x \le 1 \\ 1 - \dfrac{\rho_c}{\alpha_c (x-1)^2 + x} & x > 1 \end{cases} \tag{2}$$

$$x = \frac{\varepsilon}{\varepsilon_{c,r}}, \quad \rho_c = \frac{f_{c,r}}{E_c \varepsilon_{c,r}}, \quad n = \frac{1}{1 - \rho_c} \tag{3}$$

$$E_c = \frac{10^2}{2.2 + \dfrac{34.7}{f_{cm}}} \tag{4}$$

where d_c is the damage evolution parameter of concrete under uniaxial compression; ε is the compressive strain of concrete; α_c is the parameter for descent segment in constitutive relationship of concrete under uniaxial compression; $f_{c,r}$ is the uniaxial compressive strength of concrete and takes the representative value of the compressive strength of concrete in this paper; $\varepsilon_{c,r}$ is the peak

compressive strain corresponding to $f_{c,r}$; E_c is the elastic modulus of concrete. f_{cm} is the average value of compressive strength of concrete. The value of α_c and $f_{c,r}$ are listed in Table 1.

Table 1. Parameter values of stress-strain curves of concrete under uniaxial compression.

$f_{c,r}$ (MPa)	20	25	30	35	40	45	50	55	60	65	70	75	80
α_c	0.74	1.06	1.36	1.65	1.94	2.21	2.48	2.74	3.00	3.25	3.50	3.75	3.99
$\varepsilon_{c,r}$ (10^{-5})	147	156	164	172	179	185	192	198	203	208	213	209	224
$\varepsilon_{cu}/\varepsilon_{c,r}$	3.0	2.6	2.3	2.1	2.0	1.9	1.9	1.8	1.8	1.7	1.7	1.7	1.6

2.3. Stress-strain curve of concrete under uniaxial tension

$$\sigma = (1 - d_t) E_c \varepsilon \tag{5}$$

$$d_t = \begin{cases} 1 - \rho_t (1.2 - 0.2x^5) & x \le 1 \\ 1 - \dfrac{\rho_t}{\alpha_t (x-1)^{1.7} + x} & x > 1 \end{cases} \tag{6}$$

$$x = \frac{\varepsilon}{\varepsilon_{t,r}} \quad , \quad \rho_t = \frac{f_{t,r}}{E_c \varepsilon_{t,r}} \tag{7}$$

where d_t is the damage evolution parameter of the concrete under uniaxial tension; α_t is the parameter for descent segment in the constitutive relationship of concrete under uniaxial tension; $f_{t,r}$ is the uniaxial tension strength of concrete and takes the average value of the tension strength of concrete in this paper; $\varepsilon_{t,r}$ is the peak tensile strain corresponding to $f_{t,r}$. The value of α_t and $\varepsilon_{t,r}$ are listed in Table 2.

For different compressive strength shown in Table 3, corresponding values of α_c and $\varepsilon_{c,r}$ were acquired through linear interpolation based on the recommended information listed in Table 1. Due to the lack of experimental result, the tensile strength for different type of normal concrete was then taken as 10% of its compressive strength, which has also been adopted in Shamass R. et al. [14].

Similarly, the values of α_t and $\varepsilon_{t,r}$ were calculated with linear interpolation based on the parameter values depicted in Table 2.

Table 2. Parameter values of stress-strain curves of concrete under uniaxial tension.

$f_{t,r}$ (MPa)	1.0	1.5	2.0	2.5	3.0	3.5	4.0
$\varepsilon_{t,r}$ (10^{-6})	65	81	95	107	118	128	137
α_t	0.31	0.70	1.25	1.95	2.81	3.82	5.00

The CDP model proposed by the concrete code does not consider the influence of plastic strain on the monotonic stress-strain curve and damage evolution. In fact, the damage evolution formulas (1) and (5) are obtained by the concrete uniaxial stress-strain relationship specified in Chinese code for the design of concrete structures (GB 50010-2002), ignoring the physical background of damage evolution [16]. The disadvantage of elastic damage mechanics has been pointed out in the revised Chinese code, that it cannot fully describe the plastic deformation and hysteresis effect during material unloading and reloading [17].

The significant curve of material stress-strain during cyclic loading is not specified in the concrete specification due to the complexity of the hysteresis rule. The concrete has obvious plastic deformation under compressive stress, and the elastoplastic damage constitutive relation under uniaxial compression is generally expressed as

$$\sigma = (1 - d_{ce})\, E_c(\varepsilon - \varepsilon_p) \tag{8}$$

$$d_{ce} = \eta_d d \tag{9}$$

$$\eta_d = \frac{x(1+x)}{x(1+x)+\sqrt{x}} \tag{10}$$

where d_{ce} is the damage variable after plastic deformation; ε_p is the plastic strain.

Concrete is a quasi-brittle material, and the influence of plastic strain can be ignored under tension then the elastic damage variable is equal to the elastoplastic damage variable d_t. In addition, the calculation formula (Eq 5) is obtained by fitting the test results in the case of $d_t \leq 1$, it is may give a negative value of the damage variable. It is recommended to correct Eq 5 with reference to Eq 1.

$$d_t = \begin{cases} 1 - \dfrac{\rho_t n_t}{n_t - 1 + x^{n_t}} & x \le 1 \\ 1 - \dfrac{\rho_t}{\alpha_t (x-1)^{1.7} + x} & x > 1 \end{cases} \tag{11}$$

$$n_t = \frac{1}{1-\rho_t} \tag{12}$$

For concrete C100, the stress-strain curve of high-strength concrete under uniaxial compression (proposed by Ding et al. [18]) is used in this paper:

$$d_t = \begin{cases} \dfrac{A_1 x - x^2}{1 + (A_1 - 2)x} & x \le 1 \\ \dfrac{x}{\alpha_1 (x-1)^2 + x} & x > 1 \end{cases} \tag{13}$$

$$x = \frac{\varepsilon}{\varepsilon_o},\ y = \frac{\sigma}{f_c},\ \mathrm{A}_1 = 9.1 f_{cu}^{-4/9} \tag{14}$$

$$\alpha_1 = 2.5 \times 10^{-3} f_{cu}^3,\ \varepsilon_o = 520 f_c^{1/3} \times 10^{-6} \tag{15}$$

$$E_c = 9500 f_{cu}^{1/3} \tag{16}$$

where σ and ε are the stress and strain of concrete, respectively; f_c and ε_n are the peak stress and peak strain of concrete, respectively; α_1 is the parameter for descent segment in constitutive relationship of concrete under uniaxial compression; f_{cu} is the concrete uniaxial cube compressive strength.

2.4. Constitutive relationship of the steel rebar

An elastic-perfectly-plastic bilinear model was established to represent the constitutive relationship of the reinforcement, the yield strength f, elastic modulus E_s and Poisson ratio ν are 335 MPa, 210 GPa and 0.3, respectively.

3. Numerical simulation

In this study, the single-keyed dry joints in PCSBs tested by Jiang et al. [5] were analyzed using FE software ABAQUS, based on the model parameters discussed previously. The dimensions of the

single-keyed dry joints were 340 × 540 mm^2 with 100 mm as the thickness of the joint including a male part and a female part, as shown in Figure 5. For the single-keyed dry joints tested by Jiang et al., the specimens were identified as Mi-Vj-D-Cm-Kn, where M represented monotonic loading and the numeral following M (in this case i) indicated the confining pressure (MPa), V represented the key depth, and j was the depth size (mm), D was identified as a dry joint, C indicated concrete, m indicated concrete strength grade (MPa). Lastly, K indicated a keyed joint, and n was the number of keys.

A three-dimensional solid model was established to simulate the actual test. In the model, the concrete was simulated with solid element (C3D8R), the reinforcement was simulated with truss elements (T3D2). The damage plasticity constitutive was used for the concrete. The finite element model was shown in Figure 6. The embedded constrain was applied to the rebar and concrete. In this constrain, the translational degrees of freedom for the nodes on the rebar elements were constrained to the interpolated values of the corresponding degrees of freedom of the concrete elements. The slip and debond of the rebar were ignored. Actually, surface-to-surface contact interaction was adopted for the numerical model, with the using of finite sliding analysis procedure. Moreover, the contact surface associated with the lower portion (i.e., female part) was taken as the master surface while the other one for upper male section was defined as slave surface. Based on the experimental results [5], the friction coefficient between concrete surfaces was assumed as 0.6 for single-keyed dry joints. Particularly, material nonlinear and contact nonlinear analysis were used in the numerical simulations. Additionally, the bottom surface of the single-keyed dry joint was restrained against all translational degrees of freedom. For loading process, the confining pressure was simulated by applying constant uniform pressure on both sides of the model. The confining stress values were 1.0 and 2.0 MPa, respectively, covering the single-keyed dry joint area of 200 × 100 mm^2, as per Jiang et al. [5]. The vertical displacement-controlled loading was then applied on the top of the model, which was simulated by creating a boundary condition moving vertically downward, with a prescribed displacement rate (0.3 mm/min) as adopted in the experiments done by Jiang et al. Specially, all the slippages of joint were taken as the average deflections of that at the top and the bottom surface of the joint, which was consistent with the location of vertical LVDTs in previous experimental study.

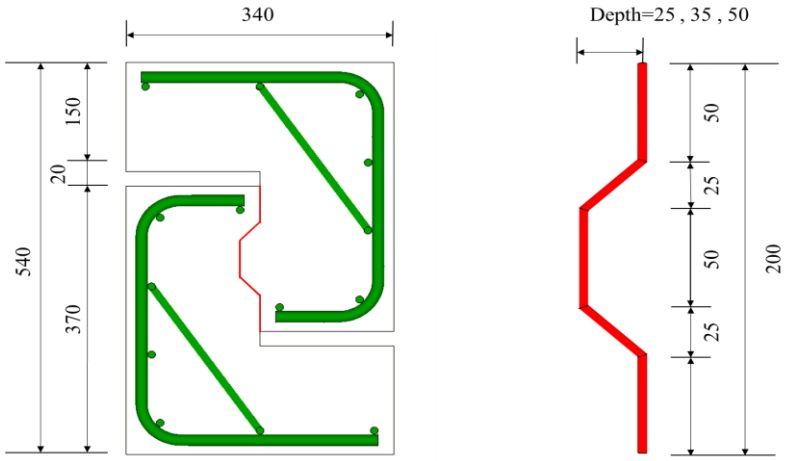

Figure 5. Dimensions of the single-keyed dry joints tested by Jiang et al. (unit: mm).

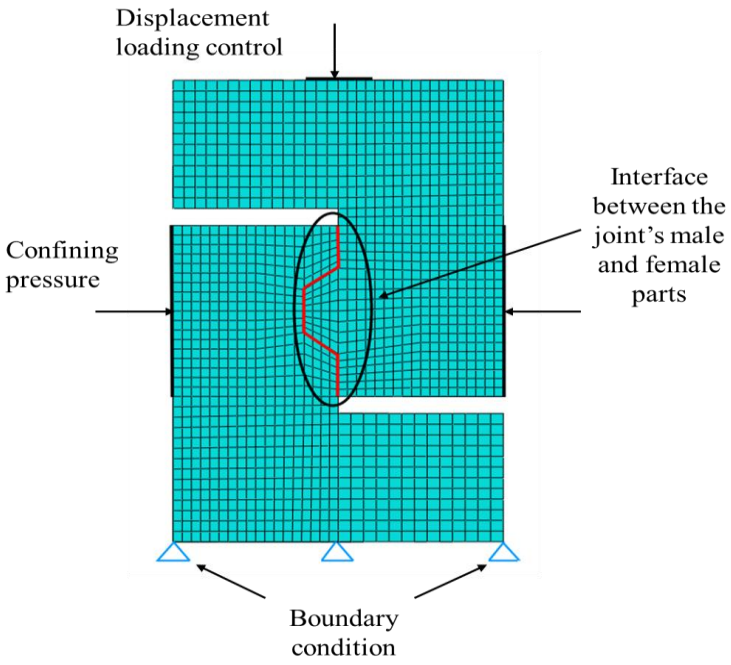

Figure 6. FE mesh, boundary conditions, and loadings for single-keyed dry joint specimens.

4. Validation of FE results

4.1. Comparison of simulation results with test results

The numerical values of the ultimate shear strength of the single-keyed dry joints were summarized in Table 3, along with the corresponding experimental values obtained by Jiang et al. [5]. The predicted ultimate shear strength for joints were all in good agreement with the corresponding experimental results. The average deviation was approximately 6%. It demonstrated that the model used in the analysis is reliable and it is generally conservative in predicting the ultimate shear strength of a single-keyed dry joint.

Table 3. Ultimate shear strength of single-keyed dry joints: experimental versus numerical.

Specimens name	Specimens tested by Jiang et al.	f_c' (Mpa)	Numerical ultimate strength V_u (kN)	Experimental ultimate strength V_t (kN)	V_u / V_t
M1.0-V25-D-C40-K1	K1-03	40.83	77.96	80.79	0.964
M1.0-V35-D-C40-K1	K1-01	41.51	86.32	89.69	0.966
M2.0-V35-D-C40-K1	K1-02	41.51	105.99	113.87	0.931
M1.0-V50-D-C40-K1	K1-04	40.83	76.64	94.47	0.811
Average value			-	-	0.918
Standard deviation			-	-	0.063

4.2. Comparisons of the load-displacement curves

Figure 7 shows the load-displacement curves from numerical analyzes of Models M1-V25-D-C40-K1, M1-V35-D-C40-K1, M1-V50-D-C40-K1 and M2-V35-D-C40-K1, which were close to the observation obtained from experiments by Jiang et al. In general, the experimental data points were distributed near the simulation curve, which indicated that those are in good agreement. The acceptable stiffness deviations in some tests probably resulted from the difference of material properties or the neglect of aggregate interlock effect of concrete under shear action. The curves in the figure can be divided into four stages: in the first (linear-elastic) stage, the relative displacement of dry joints increased with the load; in the second (plastic) stage, the stiffness of specimen began to descend, causing the slopes of the load-displacement curves decreased gradually; in the third (descending) stage, the load decreased rapidly after it reached the ultimate load, large plastic deformation and material damage were also evident. Due to the limitation of data acquisition instrument in the experiments, only the data of the ultimate load and the data after sudden dropping of the curve were recorded during the experiments. However, it should be noted that these data points were close to the numerical curves for all specimens. Thus, it was acceptable to use the simulated curves to represent the behavior of descending stage. In the last stage, i.e., the steady stage, the shear-resistance stress was provided by the residual stress after the concrete failure. The load-displacement curves predicted by the FE model also coincided with those obtained by the experiments.

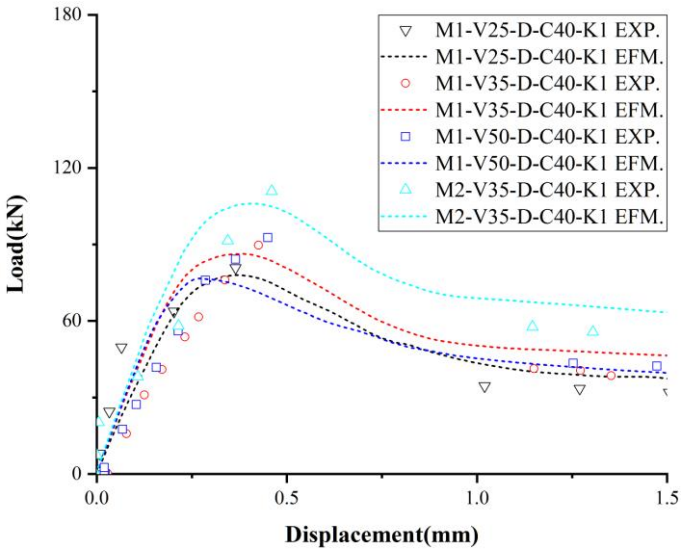

Figure 7. Comparisons of the experimental and numerical load-displacement curves for single-keyed dry joints.

4.3. Comparisons of crack propagation

Figure 8 represented the crack propagation of M1-V35-D-C40-K1 from the numerical analysis, which demonstrated the crack patterns in different stages at the applied loads of 69kN, 77kN and 86kN, respectively. These predicted crack propagations illustrated that cracking initiated at the

bottom corner of a key and propagated sideways and upward at approximately 45 °to the horizontal line, then this crack ceased to propagate. Later on, a new vertical crack, initiated from the bottom of the key and propagated upward vertically in the loading plane. It was this crack to shear off the key when it propagated to the top corner of the key. The crack propagations obtained from numerical analysis were highly similar those observed in the experiments. Comparisons indicated that the cracking pattern depicted by the FE model can reflect the cracking propagation from experimental tests (Figure 9).

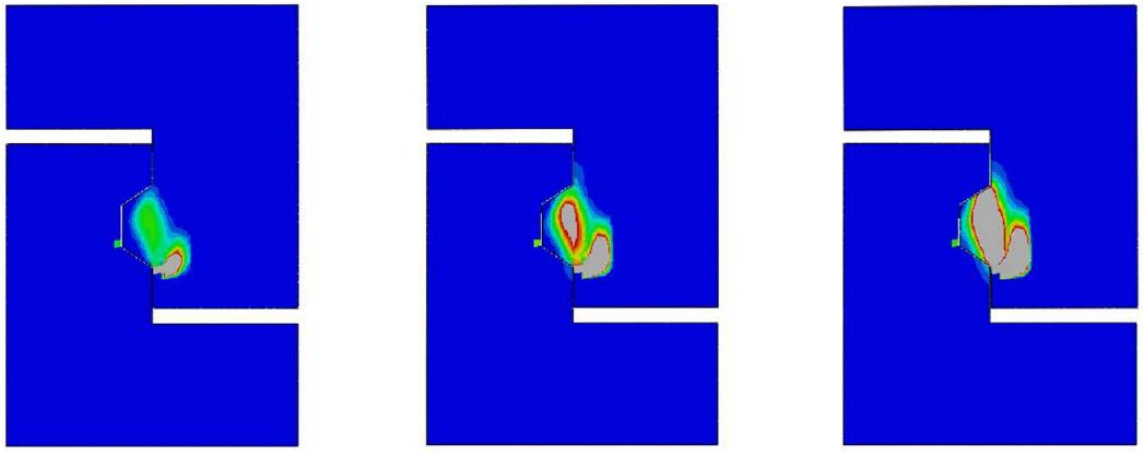

Figure 8. Crack patterns of the specimen M1-V35-D-C40-K1from numerical analyses.

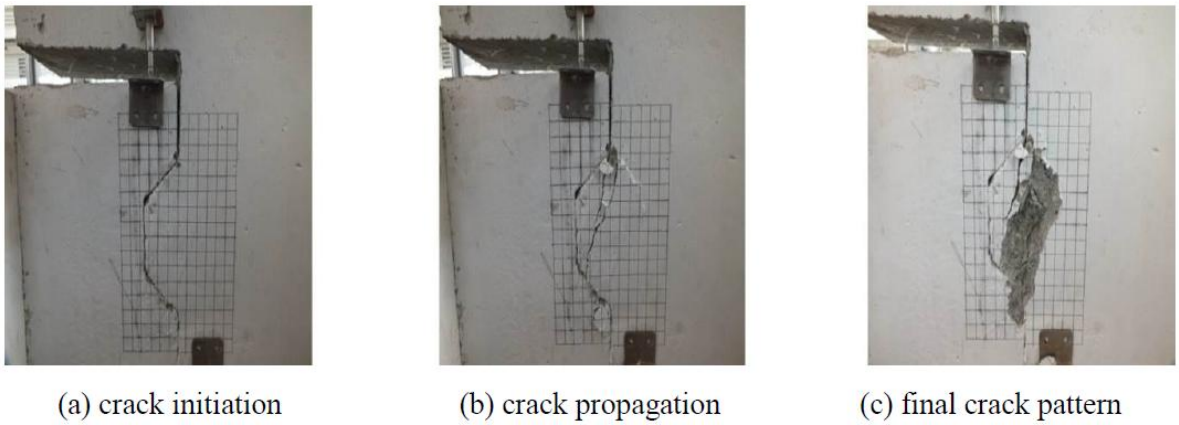

Figure 9. Crack patterns obtained from an experiment tested by Jiang et al.

5. Parametric study

The experimentally validated FE models were used for extending parametric studies on the shear behavior of single-keyed dry joints in PHCSBs, of which the main parameters were the confining pressure (0.1, 0.5, 1.0, 1.5, 2.0, 2.5, and 3.0 MPa), concrete strength (C40, C60, C80, and C100) and key depth (15 , 25, 35, 40, 45, 50 and 60 mm).

5.1. Effect of the confining pressure on the shear behavior of single-keyed dry joints

The ultimate shear strength and structural behavior of single-keyed dry joints was affected by the confining pressure. Due to the limitation of experimental tests, the horizontal confining pressure used in previous study was generally 0.5 MPa and above. In this paper, the FE models for Specimens Mi-V35-D-C40-K1, Mi-V35-D-C60-K1, Mi-V35-D-C80-K1 and Mi-V35-D-C100-K1 with the key depth of 35 mm were analyzed for the shear performance of the joints under confining pressure varying from 0.1 to 3 MPa. The numerical values of the ultimate shear strength of the single-keyed dry joints under different confining pressure are summarized in Table 4.

Table 4. Numerical results of single-keyed dry joints under different confining pressure.

Specimens	Confining pressure (MPa)	Numerical ultimate strength V_u (kN)	Relative displacement (mm)
M0.1-V35-D-C40-K1	0.1	55.47	0.248
M0.5-V35-D-C40-K1	0.5	73.95	0.412
M1.0-V35-D-C40-K1*	1.0	86.33	0.450
M1.5-V35-D-C40-K1	1.5	96.47	0.462
M2.0-V35-D-C40-K1*	2.0	106.0	0.478
M2.5-V35-D-C40-K1	2.5	115.22	0.491
M3.0-V35-D-C40-K1	3.0	124.97	0.511
M0.1-V35-D-C60-K1	0.1	65.68	0.828
M0.5-V35-D-C60-K1	0.5	92.49	0.415
M1.0-V35-D-C60-K1	1.0	103.41	0.428
M1.5-V35-D-C60-K1	1.5	115.87	0.453
M2.0-V35-D-C60-K1	2.0	125.38	0.462
M2.5-V35-D-C60-K1	2.5	134.51	0.468
M3.0-V35-D-C60-K1	3.0	144.71	0.491
M0.1-V35-D-C80-K1	0.1	71.74	1.158
M0.5-V35-D-C80-K1	0.5	118.69	0.460
M1.0-V35-D-C80-K1	1.0	122.84	0.475
M1.5-V35-D-C80-K1	1.5	133.73	0.484
M2.0-V35-D-C80-K1	2.0	145.79	0.495
M2.5-V35-D-C80-K1	2.5	156.98	0.487
M3.0-V35-D-C80-K1	3.0	159.23	0.514
M0.1-V35-D-C100-K1	0.1	82.69	0.897
M0.5-V35-D-C100-K1	0.5	132.76	0.452
M1.0-V35-D-C100-K1	1.0	137.76	0.459
M1.5-V35-D-C100-K1	1.5	149.43	0.465
M2.0-V35-D-C100-K1	2.0	158.63	0.480
M2.5-V35-D-C100-K1	2.5	169.5	0.495
M3.0-V35-D-C100-K1	3.0	178.38	0.512

Note: The numerical model with "∗" has been validated by the tests.

Figure 10 (a) shows the load-displacement curves of Specimen Mi-V35-D-C40-K1 under the confining pressure of 0.1–3.0 MPa. When the confining pressure was about 0.1 MPa, the load curve first increased with the relative displacement; then the load began to decrease after it reached the ultimate load. After that, the curve kept horizontal. For Specimen M0.5-V35-D-C40-K1, the load-displacement curve first grew linearly and then nonlinearly with a gradually-decreasing slope. The load curve decreased rapidly after it reached the ultimate load; when the curve dropped to a certain extent, it kept horizontal. As the confining pressure increased from 0.5 to 3.0 MPa, the other characteristics and trends of the curve were basically consistent except that the ultimate shear load increased correspondingly with the residual strength.

Figures 10 (b, c, and d) show the load-displacement curves of Specimens Mi-V35-D-C60-K1, Mi-V35-D-C80-K1 and Mi-V35-D-C100-K1 under the confining pressure of 0.1–3.0 MPa, respectively. For Specimens Mi-V35-D-Cm-K1 (I = 0.1, m = 60, 80, and 100), the load curves first increased with the relative displacement, and then grew nonlinearly. The curve had a small fluctuation and then slowly rose before it reached to the ultimate load. Subsequently, the curve decreased rapidly after it reached the ultimate load; Later on, the curve kept flat. For Specimens Mi-V35-D-Cm-K1 (m = 60, 80, and 100) as the confining pressure increased from 0.5 to 3.0 MPa, the load curves first increased with the relative displacement, then the load began to decrease after it reached the ultimate load, then the curve kept horizontal.

For single-keyed dry joints with 0.1 MPa confining pressure, the unusual phenomenon, as depicted in Figure 10, may also be related to the cracking process. The outward slip of upper male portion resulted in the fluctuation of loading. With the increasing of vertical load, the sliding friction became large enough to stop the slip. Meanwhile, the bottom corner crack lengthened and widened, causing the slight rotation of male part. As the loading continued, cracks in the key root area linked with each other and penetrated at last, causing the dropping of curve. This can also be observed in the figure that both the former bottom corner cracks and latter root area cracks lengthened and widened. With the aggregate interlock action along the cracking concrete, the final shear resistance of keyed joint maintained in a constant level (steady stage) at last.

Figures 11 (a, b, c, d, e, and f) show the contour plot of the maximum principal stress for the specimen Mi-V35-D-C40-K1 at the applied load of 55 kN. As the confining pressure increased, the maximum principal stress (red area) occurred at the male part of the joint decreased, therefore, most of the load was transferred onto the lower surface of the key. Interestingly, when the confining pressure increased to 3 MPa, the maximum principal stress almost disappeared at the male part of the joint. The crack would appear at the male part of the joint when the maximum principal stress reached the concrete tensile strength. The crack can be explained by the fact that this crack propagated sideways into a low stress zone in the material and thus released energy. The maximum principal stress of the specimen Mi-V35-D-C40-K1 (I = 0.1–3 MPa) were 3.036, 2.909, 2.337, 1.833, 1.639, and 1.534 MPa, respectively, which indicated that increasing confining pressure led to a high compression stress zone at the entire key area which reduced cracks running in a high stress zone and inclined the development of cracks.

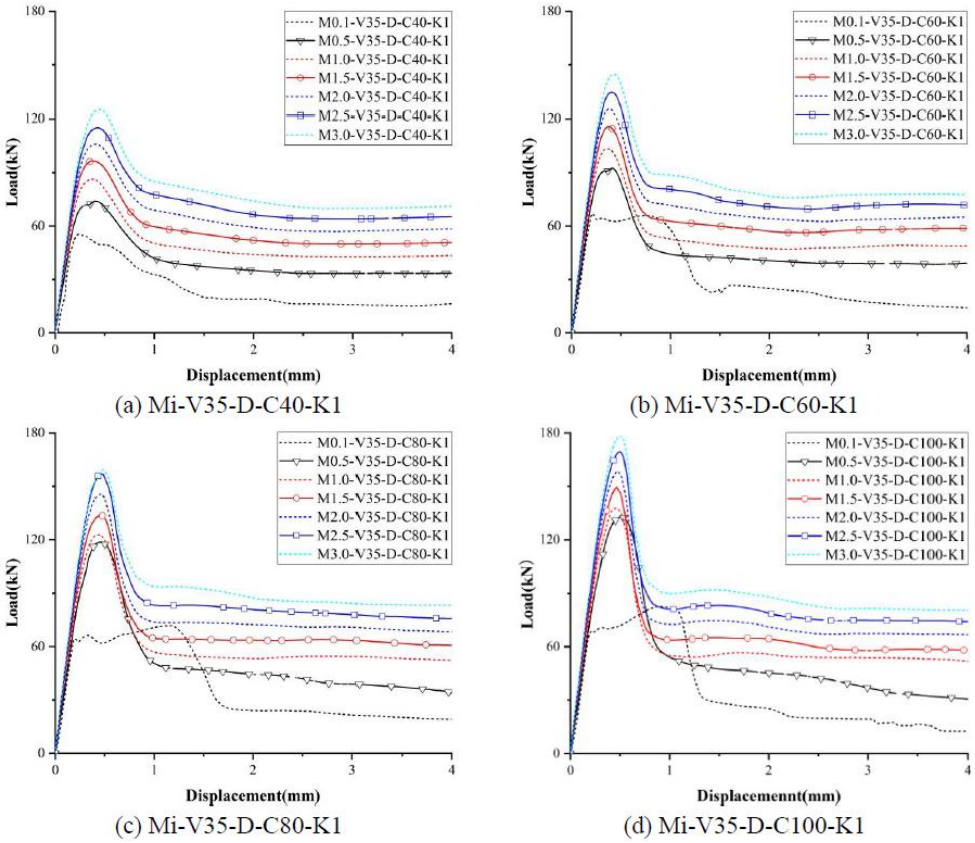

Figure 10. Load-displacement curves for single-keyed dry joints under confining pressure of 0.1–3.0 MPa.

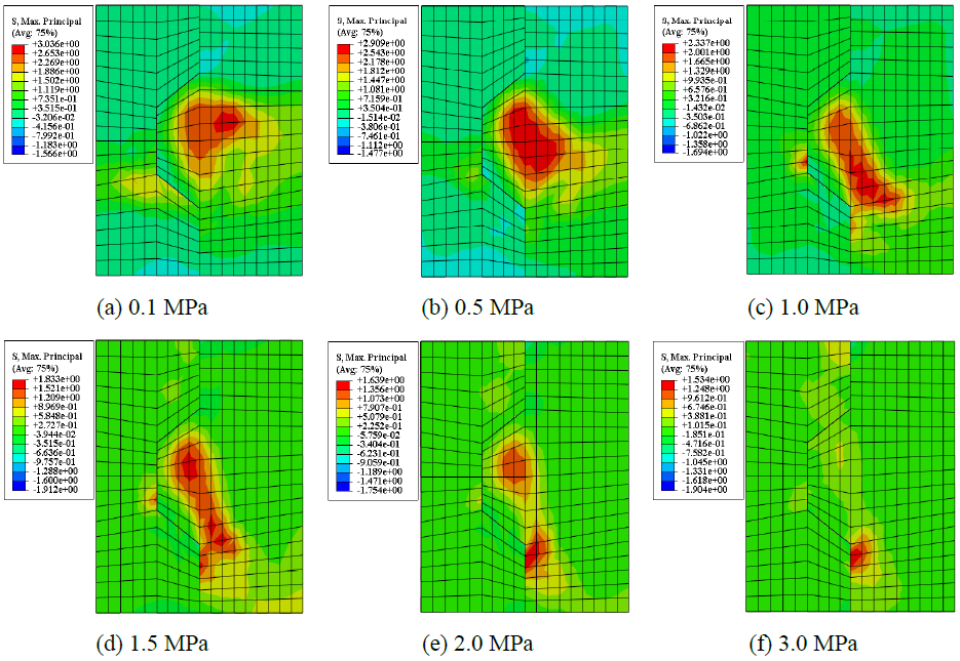

Figure 11. The contour plot of the maximum principal stress contour of specimens Mi-V35-D-C40-K1under confining pressure of 0.1–3.0 MPa.

5.2. Effect of concrete strength on the shear behavior of single-keyed dry joints

In this paper, the FE models M1-V25-D-Cm-K1, M1-V35-D-Cm-K1, M1-V45-D-Cm-K1 and M1-V60-D-Cm-K1with the confining pressure of 1.0 MPa were used to analyze the shear performance of joints under the varied concrete of C40, C60, C80 and C100. The analytical values of the ultimate shear strength of single-keyed dry joints under different concrete strength are summarized in Table 5.

Table 5. Numerical results of single-keyed dry joint specimens under different concrete strength and key depths.

Specimens	Concrete strength (MPa)	Key depth (mm)	Numerical ultimate strength V_u (kN)	Relative displacement (mm)
M1-V15-D-C40-K1	40	15	36.4	2.515
M1-V25-D-C40-K1	40	25	77.96	0.371
M1-V35-D-C40-K1	40	35	86.33	0.450
M1-V40-D-C40-K1	40	40	86.94	0.383
M1-V45-D-C40-K1	40	45	86.53	0.419
M1-V50-D-C40-K1	40	50	76.65	0.309
M1-V60-D-C40-K1	40	60	65.33	0.291
M1-V15-D-C60-K1	60	15	37.1	1.986
M1-V25-D-C60-K1	60	25	84.19	0.358
M1-V35-D-C60-K1	60	35	103.41	0.380
M1-V40-D-C60-K1	60	40	104.43	0.380
M1-V45-D-C60-K1	60	45	101.62	0.369
M1-V50-D-C60-K1	60	50	94.42	0.335
M1-V60-D-C60-K1	60	60	90.41	0.366
M1-V15-D-C80-K1	80	15	37.8	4
M1-V25-D-C80-K1	80	25	85.83	0.828
M1-V35-D-C80-K1	80	35	122.84	0.433
M1-V40-D-C80-K1	80	40	124.37	0.442
M1-V45-D-C80-K1	80	45	123.96	0.438
M1-V50-D-C80-K1	80	50	107.02	0.383
M1-V60-D-C80-K1	80	60	99.22	0.406
M1-V15-D-C100-K1	100	15	37.8	4
M1-V25-D-C100-K1	100	25	90.07	1.01
M1-V35-D-C100-K1	100	35	135.81	0.459
M1-V40-D-C100-K1	100	40	137.58	0.464
M1-V45-D-C100-K1	100	45	136.05	0.436
M1-V50-D-C100-K1	100	50	114.4	0.388
M1-V60-D-C100-K1	100	60	106.54	0.416

Note: The numerical model with "∗" has been validated by the tests.

Figure 12 (a) shows the load-displacement curves of Specimen M1-V25-D-Cm-K1 with concrete C40–C100. For concrete C40, the load curve first increased with the relative displacement, the curve grew nonlinearly and then descended steeply. Later on, the curve kept horizontal. As the concrete strength increased from C60 to C100, the load-displacement curves first linear grew. The load curves decreased rapidly after it reached the ultimate load. As the curves descend to a certain extent, the curve kept horizontal.

Figures 12 (b, c, and d) show the load-displacement curves of Specimens M1-V35-D-Cm-K1, M1-V45-D-Cm-K1 and M1-V60-D-Cm-K1 with the concrete strength C40–C100, respectively. When the concrete strength increased from C40 to C100, the load-displacement curves were generally similar except that the ultimate shear load increased correspondingly with the residual strength; the load curves first linearly and the nonlinearly increased with the relative displacement. The curves decreased rapidly after it reached the ultimate load. Subsequently, the curves kept horizontal.

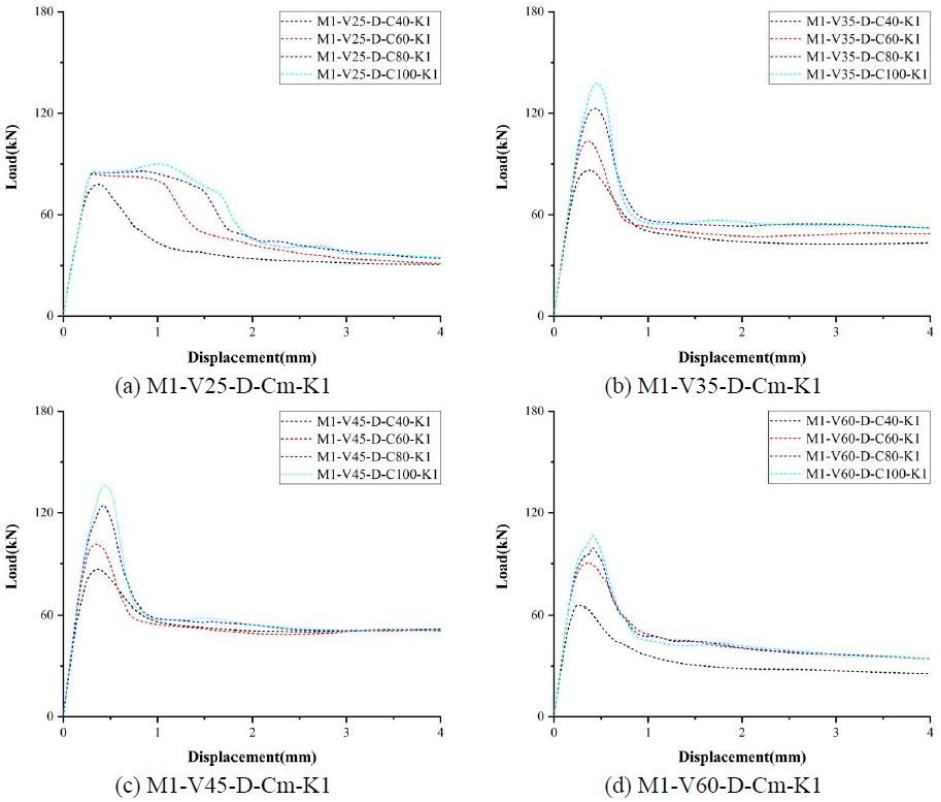

Figure 12. Load-displacement curves for single-keyed dry joints under concrete strength of C40–C100.

The above figure showed that the ultimate shear strength of single-keyed dry joint specimens increased when the concrete strength increased from C40 to C100. However, it made a small contribution to the ultimate shear capacity of dry joints under the key depth of 25 mm as the concrete strength increased from C40 to high-strength concrete C100. It had a great influence on the ultimate shear capacity of dry joints with the higher key depth as 35 mm and above, because the shear resistance of the keyed region is related to the tensile strength of concrete and the confining pressure

on the surface. When the key depth was 25 mm, the maximum principal stress of the keyed area was less than the ultimate tensile strength of high-strength concrete, only the bottom corner of the key was broken. The concrete strength had little effect on the ultimate shear capacity of the dry joints due to the key had a large slip downward. When the key depth increased to 35 mm and above, the cross-sectional area of the key increased with the key depth, the maximum principal stress of the key was higher than the ultimate tensile strength of high-strength concrete, cracks appeared at the concrete region in the male part, and the concrete strength was fully utilized. Therefore, it had a great influence on the ultimate shear strength of single-keyed dry joints when the concrete strength increased.

Figures 13 (a, b, c, and d) show the maximum principal stress contours for Specimen M1-V35-D-Cm-K1at the applied load of 75 kN. As the concrete strength increased, the maximum principal stress in the male part of the joint began to decrease, therefore, most of the load was transferred through the lower surface of the key. Increasing the concrete strength enhanced the ultimate shear strength of the model.

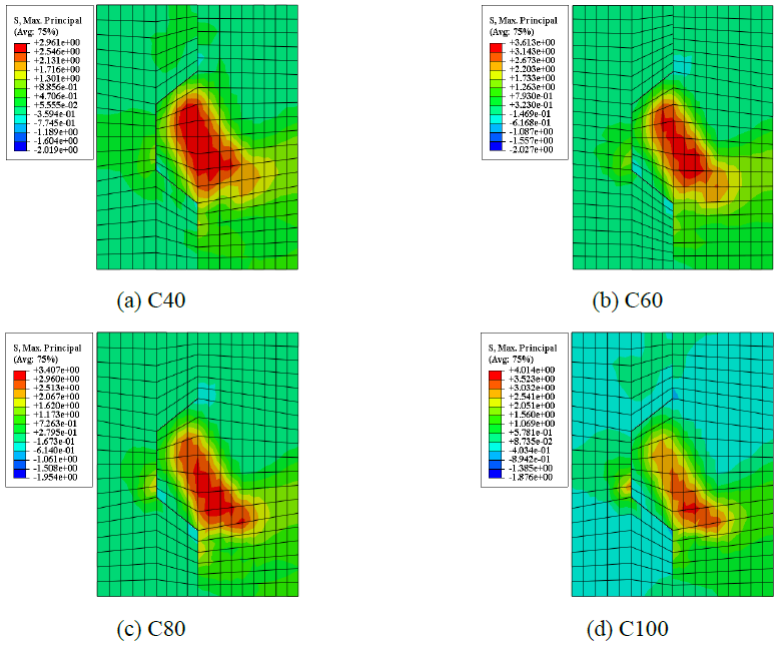

Figure 13. The contour plot of the maximum principal stress contour of specimens M1-V35-D-Cm-K1 under concrete strength of C40–C100.

5.3. Effect of key depth on the shear behavior of single-keyed dry joints

The maximum principal stress of the keyed area varies with the key size of single-keyed dry joints, which has obvious influence on the shear failure of the key. In this paper, the FE models M1-Vj-D-C40-K1, M1-Vj-D-C60-K1, M1-Vj-D-C80-K1 and M1-Vj-D-C100-K1 with the confining pressure of 1.0 MPa were analyzed for the shear performance of joints when the key depth varying from 15 to 60 mm. The analytical values of the shear strength of single-keyed dry joints for different key depth are summarized in Table 5.

Figure 14 (a) shows the load-displacement curves of Specimen M1-Vj-D-C40-K1 with the key depth of 15–60 mm. When the key depth was 15 mm, the load curve first increased with the relative displacement, and then the vertical relative slip continued to increase, but the curve no longer rose and remained horizontal. As the key depth increased from 25 to 40 mm, the load-displacement curves were generally consistent except that the ultimate shear load increased correspondingly with the residual strength. The curve first linearly grew and slowly rose to the ultimate load. The load curve decreased rapidly after it reached the ultimate load. Later on, the curve kept horizontal. The load-displacement curves of the specimen under the key depth from 40 to 60 mm was basically consistent with those for the key depth from 25 to 40 mm except that the ultimate shear load decreased correspondingly with the residual strength.

Figures 14 (b, c, and d) show the load-displacement curves of Specimens M1-Vj-D-C60-K1, M1-Vj-D-C80-K1 and M1-Vj-D-C100-K1 with the key depth of 15–60 mm, respectively. When the key depth was 15 mm, the load curves first increased with the relative displacement, and then the curve no longer rose and remained horizontal. When the key depth was 25 mm, the load curve first increased with the relative displacement, and then the curve slowly rose before it reached to the ultimate load. Subsequently, the curve decreased after it reached the ultimate load and then kept horizontal. In addition, the load-displacement curves of the specimens with the key depth from 35 to 60 mm were basically consistent with Specimen M1-Vj-D-C40-K1 except that the ultimate shear load decreases correspondingly with the residual strength.

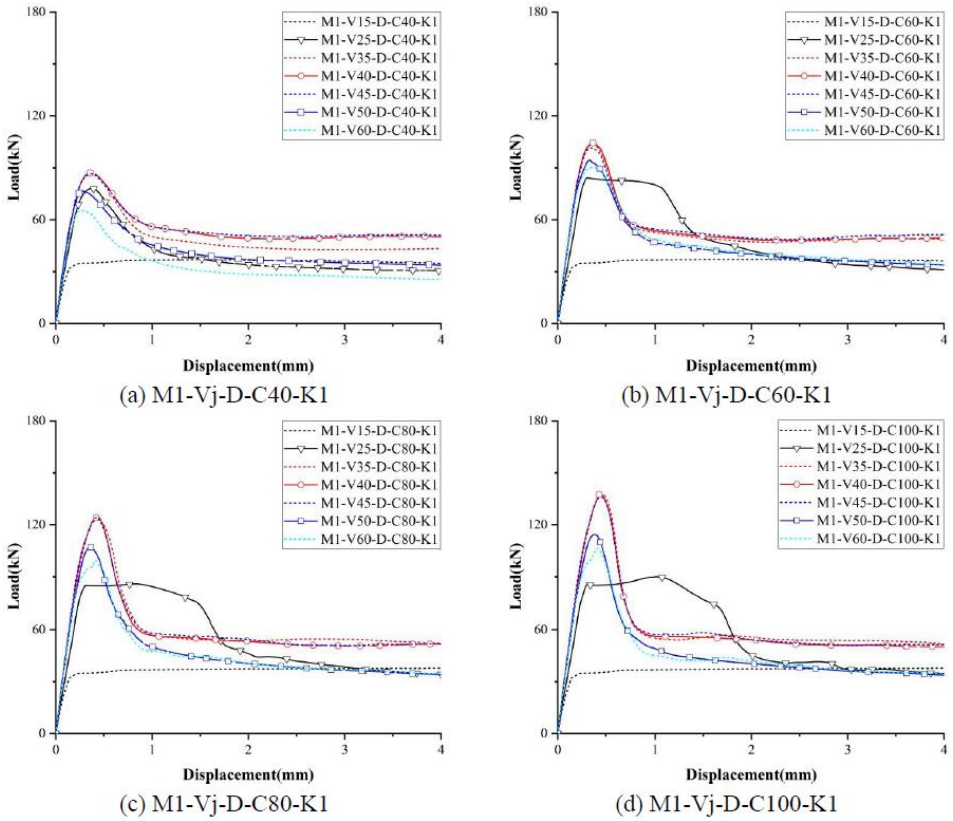

Figure 14. Load-displacement curves for single-keyed dry joint specimens under key depth of 15–60 mm.

Figures 15 (a, b, c, and d) show the maximum principal stress contour for the specimen M1-Vj-D-C60-K1 with the key depth of 15–60 mm under the applied load of 75 kN. The contourplot of the maximum principal stress of the model significantly changed for the different key depth. The maximum principal stress in the male part of the joint decreased when the key depth increased from 25 to 40 mm. However, the maximum principal stress mainly concentrated on the bottom corner of the key when the key depth increased from 40 to 60 mm, and the red area gradually increased. The maximum principal stress of the specimen M1-Vj-D-C60-K1 (j = 25–60 mm) was 3.474, 3.449, 3.150, 3.372, 3.544, and 3.742 MPa, respectively. It can be concluded that the key depth of 40 mm is the optimal size for the single-keyed dry joints, which minimizes the maximum principal stress of the shear zone.

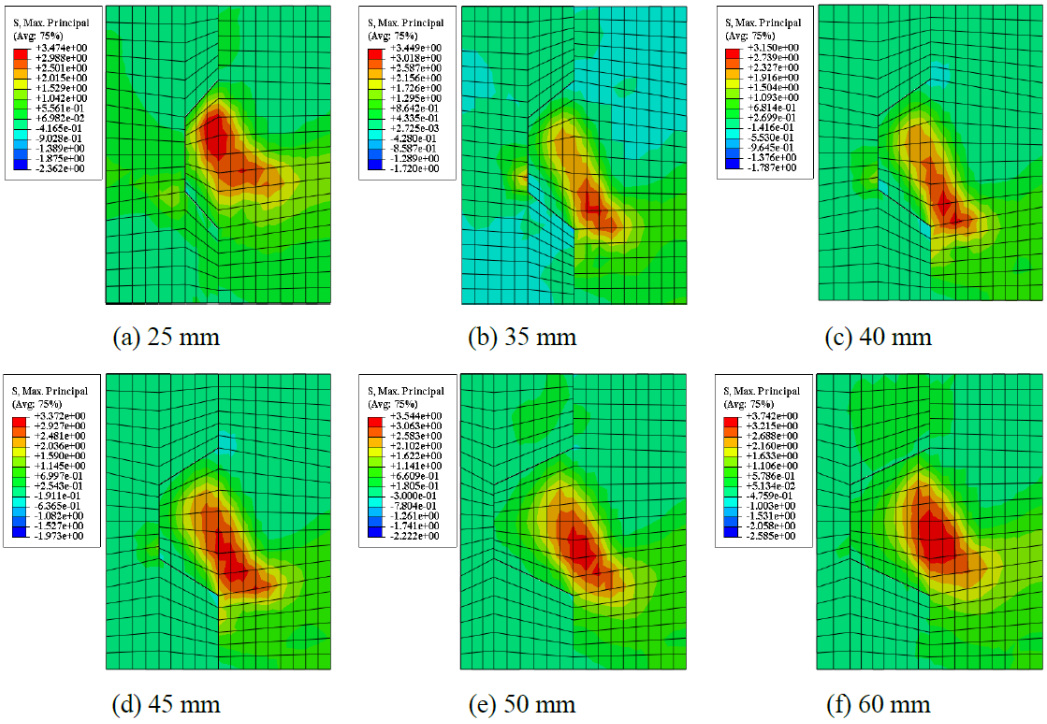

Figure 15. The contour plot of the maximum principal stress contour of specimens M1-Vj-D-C60-K1 under key depth of 15–60 mm.

6. Comparisons with the AASHTO formula

Currently, the design for the shear capacity of dry joints was usually based on AASHTO 2003 specification [19], which is:

$$V_j = A_K \sqrt{6.792\times10^{-3} f_c'}(12 + 2.466\sigma_n) + 0.6A_{sm}\sigma_n (MN) \tag{17}$$

where A_K is the area of all base of keys in the failure plane (m^2), f_c' is the compressive strength of concrete (MPa), σ_n is the normal compressive stress in concrete after allowance for all

prestress loss determined at the centroid of the cross section (MPa); A_{sm} is the area of contact between smooth surfaces on the failure plane (m^2).

The shear capacity of the keyed dry joint in PHCSBs obtained from numerical analyses and the AASHTO formula (Eq 17), under different values of confining pressure, concrete strength and key depth was illustrated in Table 6. The average values of V_u / V_a for single-keyed dry joints under different confining pressure, concrete strength and key depth were 1.01, 1.13 and 0.89, respectively. Here, V_u is the numerical result, and V_a is the AASHTO result. It can be seen that the AASHTO formula predicts the shear strength of single-keyed dry joints conservatively for almost all specimens.

Table 6. Comparisons of AASHTO calculations with parametric analysis results.

Cases	Specimens	Numerical results V_u （kN）	AASHTO V_a （kN）	V_u / V_a	Average		Standard deviation	
Confining pressure	M0.1-V35-D-C40-K1	55.47	65.63	0.85	1.01	1.01	0.07	0.11
	M0.5-V35-D-C40-K1	73.95	73.26	1.01				
	M1.0-V35-D-C40-K1	86.33	82.81	1.04				
	M1.5-V35-D-C40-K1	96.47	92.36	1.04				
	M2.0-V35-D-C40-K1	106.0	101.91	1.04				
	M2.5-V35-D-C40-K1	115.22	111.45	1.03				
	M3.0-V35-D-C40-K1	124.97	121.0	1.03				
Concrete strength	M1.0-V35-D-C40-K1	86.33	82.81	1.04	1.13		0.05	
	M1.0-V35-D-C60-K1	103.41	89.2	1.16				
	M1.0-V35-D-C80-K1	122.84	105.75	1.16				
	M1.0-V35-D-C100-K1	137.76	119.1	1.16				
Key depth	M1.0-V15-D-C40-K1	36.4	82.81	0.44	0.89		0.20	
	M1.0-V25-D-C40-K1	77.96	82.81	0.94				
	M1.0-V35-D-C40-K1	86.33	82.81	1.04				
	M1.0-V40-D-C40-K1	86.94	82.81	1.05				
	M1.0-V45-D-C40-K1	86.53	82.81	1.04				
	M1.0-V50-D-C40-K1	76.65	82.81	0.93				
	M1.0-V60-D-C40-K1	65.33	82.81	0.79				

Figure 16 shows the shear capacity of the single-keyed dry joints obtained from the numerical analyses conducted on Mi-V35-D-C40-K1 with that estimated using the AASHTO formula under various confining pressure. The results were almost identical under high values of confining pressure; however, the numerical results and AASHTO results had a large deviation for the confining pressure of 0.1 MPa. Due to the bottom of joints is more likely to open in low confining pressure, this decreases the ultimate load of joints because of the weakening of both friction and shear resistance. The AASHTO specification recommended that the formula for the shear strength of single-keyed dry

joints, however, the influence of this disadvantageous phenomenon was not considered in the calculation of the shear keys.

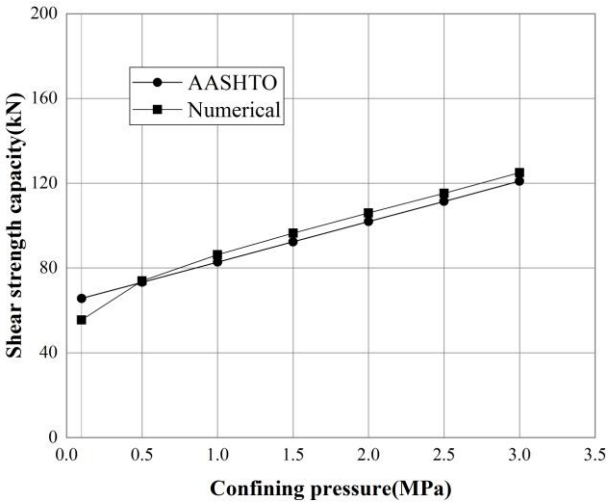

Figure 16. Ultimate shear strength of Specimens Mi-V35-D-C40-K1 from numerical analysis and the AASHTO formula for various confining pressure.

Figure 17 shows the shear capacity of the single-keyed dry joints obtained from numerical analyses of M1.0-V35-D-Cm-K1 with that estimated using the AASHTO formula for various concrete strength. It can be seen that the AASHTO formula predicted the ultimate shear strength of single-keyed dry joints with lower concrete strength well when compared with numerical results. AASHTO formula conservatively predicted the ultimate shear strength of single-keyed dry joints with high-strength concrete.

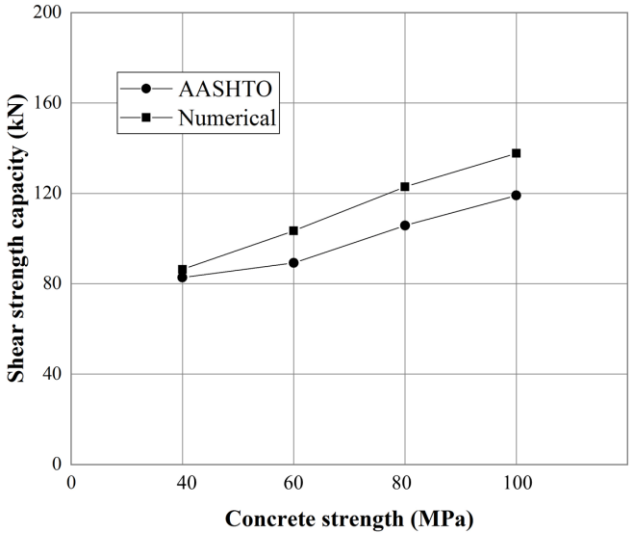

Figure 17. Ultimate shear strength of Specimens M1.0-V35-D-Cm-K1 from numerical analysis and the AASHTO formula for various concrete strength.

Figure 18 shows the shear capacities of single-keyed dry joints obtained from numerical analyses of M1.0-Vj-D-C40-K1with that estimated using the AASHTO formula under various values of key depth. The AASHTO specification recommended that the key depth should be greater than 2 times the maximum aggregate particle size of the concrete and not less than 35 mm, however, the influence of the key depth was not considered in the design of the shear keys. It can be seen that the AASHTO formula overestimated the ultimate shear strength of single-keyed dry joints with key depth of 15, 25, 50, and 60 mm when compared with numerical results, it underestimated the ultimate shear capacity of single-keyed dry joints under the key depth of 35, 40, and 45 mm. The calculated ultimate shear capacity by AASHTO formula was constant, which cannot accurately predicting the shear strength of single-keyed dry joints with different depth. This study suggests that 40 mm is the optimal design depth for single-keyed dry joints. The shear behavior of single-keyed dry joints with different key depth should be explored further in future.

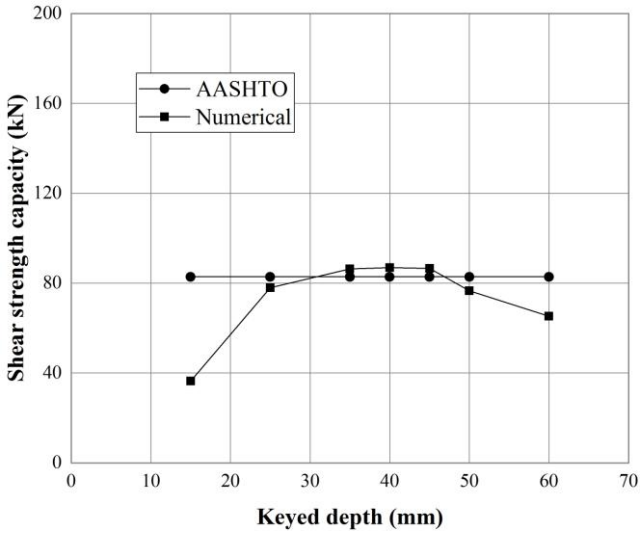

Figure 18. Ultimate shear strength of Specimens M1.0-Vj-D-C40-K1 from numerical analysis and the AASHTO formula for various key depth.

7. Conclusions

This study has investigated the behavior of single-keyed dry joints in PHCSBs based on validated FE analyses. The numerical results were presented in the ultimate shear strength of single-keyed dry joints, load-displacement curves, crack pattern, and failure mode. The validated numerical model was then used for parametric studies, focusing on the effects of the confining pressure, concrete strength and key depth on the shear behavior of single-keyed dry joints in PHCSBs. The main conclusions are:

(1) The FE results were in good agreement with the experimental results in terms of crack propagation, load-displacement relationship, suggesting that the proposed model was accurate and reliable enough to predict the shear behavior of single-keyed dry joints. The deviation in the ultimate shear strength was less than 6%. The FE model can be used conveniently to simulate the shear behavior of single-keyed dry joints in PHCSBs.

(2) The load-displacement curves of the single-keyed dry joints in PHCSBs increased approximately linearly before the cracking started. After concrete cracking, the stiffness of specimens began to descend, causing the slope of the load-displacement curve decreasing gradually, and then the load decreased rapidly after it reached the ultimate load. Large plastic deformation and material damage were also evident. Later on, the curve became horizontal.
(3) The ultimate shear strength of the single-keyed dry joints in PHCSBs increased with the confining pressure. In addition, the concrete strength had a significant effect on the shear strength of single-keyed dry joints in PCSBs.
(4) The ultimate shear strength of single-keyed dry joints in PCSBs increased when the key depth increased from 15 to 40 mm; however, it decreased when the key depth increased from 40 to 60 mm. It can be concluded that the key depth of 40 mm was the optimal design depth for single-keyed dry joints. When the key depth was 25 mm, the key would not be damaged, and the key of the joints slipped, thus, the concrete strength had little effect on the ultimate shear strength of single-keyed dry joints.
(5) The ultimate shear capacity was low when single-keyed dry joints under the confining pressure of 0.1 MPa and small key depth. The shear ultimate load of the specimen M1.0-V35-D-C60-K1 was 158% that of the specimen M0.1-V35-D-C60-K1 with the confining pressure of 0.1 MPa. The shear ultimate load of the specimen M1-V35-D-C60-K1 with key depth of 35 mm was 278% that of the specimen M1-V15-D-C60-K1 with key depth of 15 mm.
(6) The AASHTO formula may conservatively predict the ultimate shear capacity of single-keyed dry joints in PHCSBs. However, it underestimated the ultimate shear strength of single-keyed dry joints of high-strength concrete and overestimated the ultimate shear strength of single-keyed dry joints with the key depth of 15, 25, 50, and 60 mm.

Acknowledgements

This research was funded by National Natural Science Foundation of China (No. 51778150), Natural Science Foundation of Guangdong Province, China (No. 2016A030313699) and Science and Technology Planning Project of Guangzhou City, China (No. 201804010422). The authors gratefully acknowledge these generous supports and declare that they have no conflict of interests.

Conflict of interest

All authors declare no conflict of interest in this paper.

References

1. K. Koseki and J. E. Breen, Exploratory study of shear strength of joints for precast segmental bridges, *Dryness*, (1983).
2. A. C. Aparicio, G. Ramos and J. R. Casas, Testing of externally prestressed concrete beams, *Eng. Struct.*, **24** (2002), 73–84.
3. J. Turmo, G. Ramos and A. C. Aparicio, Shear strength of match cast dry joints of precast concrete segmental bridges: proposal for Eurocode 2, *Mater. Construcc.*, **56** (2006), 45–52.

4. H. Jiang, Y. Chen, A. Liu, et al., Effect of high-strength concrete on shear behavior of dry joints in precast concrete segmental bridges, *Steel Compos. Struct.*, **22** (2016), 1019–1038.
5. H. Jiang, L. Chen, Z. J. Ma, et al., Shear behavior of dry joints with castellated keys in precast concrete segmental bridges, *J. Bridge Eng.*, **20** (2015), 04014062.
6. H. Jiang, R. Wei, Z. J. Ma, et al., Shear strength of steel fiber-reinforced concrete dry joints in precast segmental bridges, *J. Bridge Eng.*, **21** (2016), 04016085.
7. C. L. Roberts, J. E. Breen and M. E. Kreger, Measurement based revisions for segmental bridge design and construction criteria, *Bridge Design*, (1993).
8. J. Turmo, G. Ramos and A. C. Aparicio, Shear strength of dry joints of concrete panels with and without steel fibres: Application to precast segmental bridges, *Eng. Struct.*, **28** (2006), 23–33.
9. X. Zhou, N. Mickleborough and Z. Li, Shear strength of joints in precast concrete segmental bridges, *ACI Struct. J.*, **102** (2005), 901–904.
10. T. H. Kim, Y. J. Kim, B. M. Jin, et al., Numerical study on the joints between precast post-tensioned segments, *Int. J. Concr. Struct. M.*, **19** (2007), 3–9.
11. M. Alcalde, H. Cifuentes and F. Medina, Influence of the number of keys on the shear strength of post-tensioned dry joints, *Mater. Construcc.*, **63** (2013), 297–307.
12. R. Shamass, X. Zhou and Z. Wu, Numerical analysis of shear-off failure of keyed epoxied joints in precast concrete segmental bridges , *J. Bridge Eng.*, **22** (2017), 04016108.
13. P. Kmiecik and M. Kamiński, Modelling of reinforced concrete structures and composite structures with concrete strength degradation taken into consideration, *Arch. Civ. Mech. Eng.*, **11** (2011), 623–636.
14. R. Shamass, X. Zhou and G. Alfano, Finite-element analysis of shear-off failure of keyed dry joints in precast concrete segmental bridges, *J. Bridge Eng.*, **20** (2014), 04014084.
15. GB50010-2010, *Code for design of concrete structures*, Ministry of Housing and Urban-Rural Development of China, Beijing, (2010).
16. GB50010-2002, *Code for design of concrete structures*, Ministry of Housing and Urban-Rural Development of China, Beijing, (2002).
17. X. Ren and J. Li, Calculation of concrete damage and plastic deformation, *Building Struct.*, **45** (2015), 29–31.
18. Z. Yu and F. Ding, Unified calcuation method compression mechanical properties of concrete, *J. Building Struct.*, **24** (2003), 41–46.
19. AASHTO, *Guide specifications for design and construction of segmental concrete bridges*, 2nd Ed., Washington, DC, 92, (2003).

AIMS Press